Langmuir

Article

pubs.acs.org/Langmuir

# Electroosmosis in a Finite Cylindrical Pore: Simple Models of End Effects

J. D. Sherwood,[*,†] M. Mao,[‡] and S. Ghosal[‡,§]

[†]Department of Applied Mathematics and Theoretical Physics, University of Cambridge,Wilberforce Road, Cambridge, CB3 0WA, United Kingdom

[‡]Department of Mechanical Engineering and [§]Department of Engineering Sciences and Applied Mathematics, Northwestern University, 2145 Sheridan Road, Evanston, Illinois 60208, United States

**ABSTRACT:** A theoretical model of electroosmosis through a circular pore of radius $a$ that traverses a membrane of thickness $h$ is investigated. Both the cylindrical surface of the pore and the outer surfaces of the membrane are charged. When $h \gg a$, end effects are negligible, and the results of full numerical computations of electroosmosis in an infinite pore agree with theory. When $h = 0$, end effects dominate, and computations again agree with analysis. For intermediate values of $h/a$, an approximate analysis that combines these two limiting cases captures the main features of computational results when the Debye length $\kappa^{-1}$ is small compared with the pore radius $a$. However, the approximate analysis fails when $\kappa^{-1} \gg a$, i.e., when the charge cloud due to the charged cylindrical walls of the pore spills out of the ends of the pore, and the electroosmotic flow is reduced. When this spilling out is included in the analysis, agreement with computation is restored.

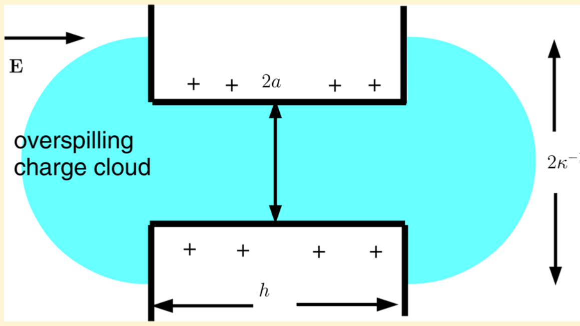


## 1. INTRODUCTION

Electroosmosis in a circular cylindrical pore of finite length $h$ differs from that in an infinitely long pore due to end effects. If the cylinder length $h = 0$, then the pore consists of a hole in a charged membrane of zero thickness, and electroosmosis can be considered to be entirely due to end effects. This case was considered by us previously.[1] When the cylindrical pore is infinitely long, end effects are negligible, and the computation of the electroosmotic volumetric flow rate $Q$, for arbitrary Debye lengths and surface charge densities, is standard[2,3] (with similar results available for infinitely long planar channels[4,5]). Here, we are interested in intermediate values of $h$.

Full numerical computation of the Poisson−Nernst−Planck (PNP) equations for ionic motion is, of course, possible, and some typical results were reported by Mao et al.[1] Such numerical computations, however, do not identify the mechanisms underlying the qualitative features of the physical system. Here, we discuss how simple models, based on continuity of electric current and volumetric flow rate, can be combined in order to estimate end effects for pore lengths $h > 0$. We assume that the zeta potential on the surface of the membrane is small, so that the Poisson−Boltzmann equation governing the equilibrium charge cloud can be linearized, and the electroosmotic velocity can be determined by an analysis equivalent to that of Henry[8] for electrophoresis, i.e., fluid motion is generated by the effect of the applied electric field acting on the equilibrium charge cloud (which is not deformed either by the applied electric field or by fluid motion). In this limit, the electroosmotic volumetric flow rate $Q$ through the hole in the membrane can be determined by means of the reciprocal theorem.[1]

Figure 1 shows the axisymmetric geometry that we are considering. The cylindrical pore CD has radius $a$ and length $h$.

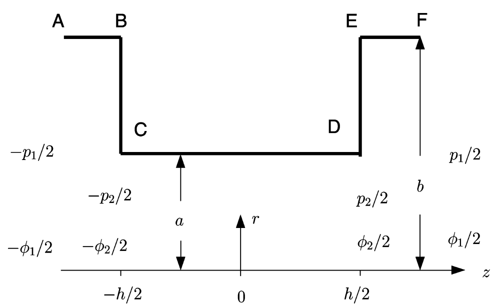


**Figure 1.** Cylindrical pore CD, of length $h$ and radius $a$ with surface charge density $\sigma_c$, passing through the membrane with surface charge density $\sigma_m$ on the two surfaces BC and DE. The reservoirs on either side of the membrane are large ($b \gg a$). The pore and reservoirs are axisymmetric about the $z$ axis.

The cylindrical surface CD of the pore has surface charge density $\sigma_c$, and the membrane surfaces BC and DE have surface charge density $\sigma_m$. An electrical potential difference is applied betwen the fluid reservoirs at either side of the membrane, and electroosmotic flow is generated by the resulting electric field

**Received:** March 6, 2014

acting on the charge cloud adjacent to the charged surfaces. The analysis of Mao et al.[1] assumed that the external reservoirs on either side of the pore were unbounded, with radius $b = \infty$. For the numerical computations presented in section 3, the external reservoirs were bounded by uncharged cylinders of radius $b \gg a$, sufficiently large that numerical results when $h = 0$ differed little from the analytic results for $h = 0$ and $b$ infinite. There have been many studies in which flow is generated in cylinders of different dimensions, connected either in series[9] or in networks intended to represent porous media.[10] Here, however, we are interested in the effect of the surfaces BC and DE of the membrane on electroosmotic flow within the cylindrical pore, and any boundaries, AB and EF, of the external reservoirs are so far away that they can be neglected.

We shall allow the surface charge density $\sigma_m$ on the membrane to differ from the charge density $\sigma_c$ on the wall of the cylindrical pore. There have been previous detailed studies of the effect of a discontinuity in surface charge density on electroosmosis.[11,12] The fine details of the charge cloud and fluid motion around such a discontinuity will be lost by the simple models presented here. They are, of course, fully taken into account in the numerical computations discussed in section 3.

In section 2, we set up the approximate analysis of end effects and compare results to those obtained from full numerical computations. The analysis is presented from first principles, but it can alternatively be set within the framework of the reciprocal theorem, as explained in section 2.6. The agreement between the approximate analysis and full computation is, in general, good, except for large Debye lengths $\kappa^{-1} \gg a$. In section 4, we consider this case in more detail in order to evaluate how much of the charge cloud due to the charged walls of the cylindrical pore lies within the pore and how much spills out beyond the ends of the pore. When this overspill is taken into account, the agreement between the computations and the approximate model is improved.

## 2. COMPOSITE ELECTROOSMOTIC COEFFICIENT

**2.1. Pore Geometry.** The axisymmetric geometry that we are considering is shown in Figure 1. We use cylindrical polar coordinates $(r,z)$, with the $z$ axis along the axis of symmetry and $z = 0$ at the midpoint of the cylindrical pore, the ends of which are at $z = \pm h/2$. When $h = 0$, we shall also use oblate spherical coordinates $(\xi,\eta)$, with

$$z = a \sinh \xi \cos \eta, \quad r = a \cosh \xi \sin \eta \tag{1}$$

where $-\infty < \xi < \infty$ and $0 \leq \eta < \pi/2$.

The cylindrical pore and the reservoirs at either end are filled with liquid with electrical conductivity $\Sigma$ and viscosity $\mu$. The wall CD of the cylindrical pore is charged, with uniform surface charge density $\sigma_c$, and the surface charge density over the membrane surfaces, BC and DE, is $\sigma_m$. The electrical permittivity $\epsilon_s$ of the membrane will be typically much smaller than the permittivity $\epsilon$ of the liquid, and we assume $\epsilon_s = 0$. We assume that the reservoir boundaries AB and EF are uncharged and at infinity. We shall occasionally refer to the surface potential $\zeta$, which will not, in general, be uniform, but which is required to be small, with $\zeta \ll kT/e$, where $e$ is the elementary charge and $kT$, the Boltzmann temperature. The electrical potential $\phi_0$ within the equilibrium charge cloud therefore satisfies the linearized Poisson−Boltzmann equation so that

$$\nabla^2 \phi_0 = \kappa^2 \phi_0 \tag{2}$$

where $\kappa^{-1}$ is the Debye length, and the charge density in the equilibrium charge cloud is

$$\rho_0 = - \in \kappa^2 \phi_0 \tag{3}$$

## 2. THE APPLIED ELECTRIC FIELD

The applied electric field is $\mathbf{E} = -\nabla\chi$, where the potential $\chi$ satisfies the Laplace equation

$$\nabla^2 \chi = 0 \tag{4}$$

with gradient

$$\mathbf{n}.\ \nabla \chi = 0 \tag{5}$$

normal to the walls of the membrane and of the cylindrical pore. In $z > 0$, the electric potential far from the membrane is $\chi = \phi_1/2$, and the potential far from the membrane in $z < 0$ is $\chi = -\phi_1/2$.

When the membrane thickness $h = 0$, the potential can be expressed explicitly as[13]

$$\chi = \frac{\phi_1}{2}\left[1 - \frac{2}{\pi}\tan^{-1}\left(\frac{1}{\sinh \xi}\right)\right] = \tilde{\chi}_m(r, z)\phi_1 \tag{6}$$

On the plane of the membrane, within the circular opening,

$$\tilde{\chi}_m = 0, \quad z = 0, r < a, h = 0 \tag{7}$$

The liquid within the pore has electrical conductivity $\Sigma$; we have assumed that surface charge density (and hence the density of charge in the cloud of counterions) is small, so that surface conductivity may be neglected. Indeed, if the mobilities of the various ionic species are identical, then the surface conductivity due to the mobile charge cloud given by the linearized model (2) at $O(e\zeta/kT)$ is zero. The total electric current $I_m$ flowing through the hole in the membrane is therefore

$$I_m = -\frac{\phi_1}{R_m}, \quad R_m = \frac{1}{2a\Sigma} \tag{8}$$

If $h > 0$, then we assume that the potential within the cylindrical pore varies linearly and approximate the potential within the pore as

$$\chi = \tilde{\chi}_c \phi_2 = \frac{z}{h}\phi_2, \quad r < a, |z| < h/2 \tag{9}$$

as would be expected in the absence of any end effects. The potential in $z > h/2$ is approximated by that outside a membrane (with a hole) of zero thickness

$$\chi = \frac{\phi_2}{2} + (\phi_1 - \phi_2)\tilde{\chi}_m(r, z - h/2) \tag{10}$$

with $\chi(r,z) = -\chi(r,-z)$. This approximation (9 and 10) is continuous at $z = \pm h/2$ where the potential is assumed to be $\pm\phi_2/2$ across the entire width of the opening (by eq 7). The as yet unspecified potential $\phi_2$ is determined by requiring continuity of the electrical current at $z = \pm h/2$. The current $I_c$ through the cylindrical pore is

$$I_c = -\frac{\phi_2}{R_c}, \quad R_c = \frac{h}{\pi a^2 \Sigma} \tag{11}$$

and the electrical current through the reservoir in $z > h/2$ is, by eq 8,

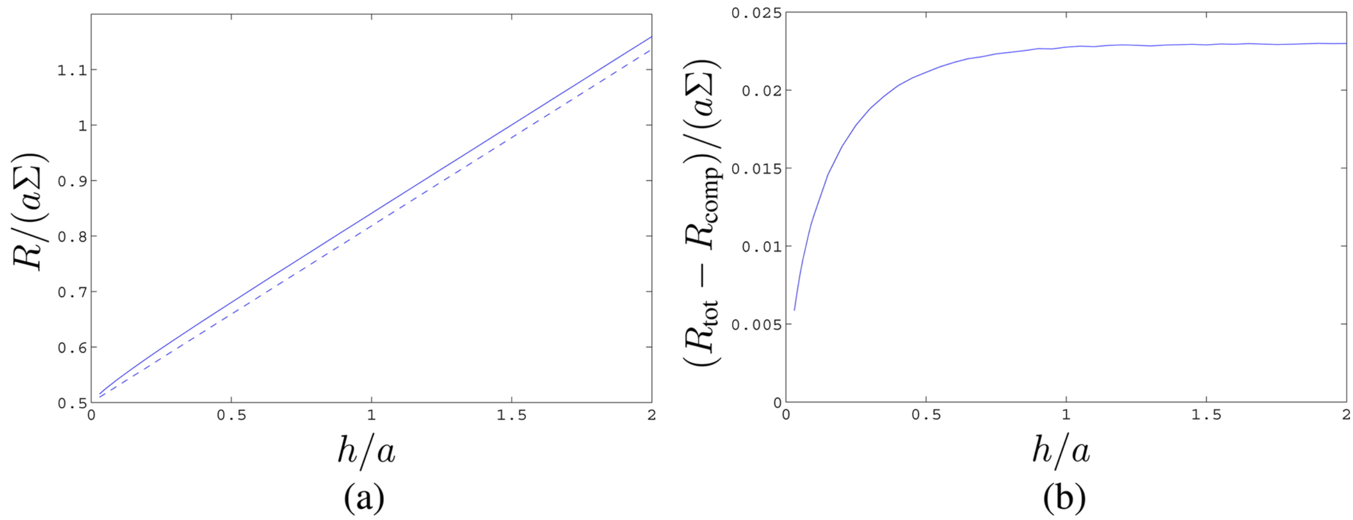


**Figure 2.** (a) Nondimensional Ohmic resisistance $R/(a\Sigma)$ of a hole of radius $a$ in a membrane of thickness $h$, as a function of $h/a$. Solid line, $R_{tot}/(a\Sigma)$ computed numerically; dashed line, the approximation $R_{comp}/(a\Sigma)$ (14). (b) The difference $(R_{tot} - R_{comp})/(a\Sigma)$.

$$I_m = -\frac{\phi_1 - \phi_2}{R_m} \tag{12}$$

Equating $I_c$ (11) and $I_m$ (12), we find

$$\phi_2 = \frac{R_c\phi_1}{R_m + R_c} \tag{13}$$

This computation suggests that the system can be treated as two resistors in series, with composite resistance

$$R_{comp} = R_m + R_c \tag{14}$$

However, this estimate assumes a uniform potential over the ends of the pore at $z = \pm h/2$, and we have effectively inserted thin, perfectly conducting sheets over the pore ends. Removal of these sheets can only increase the resistance and hence $R_{comp}$ is an underestimate for the true total resistance $R_{tot}$. Figure 2a shows $R_{tot}/(a\Sigma)$ computed numerically by means of the Freefem++ finite element package,[14] together with $R_{comp}/(a\Sigma)$. The difference is small and is shown in Figure 2b.

**2.3. Electroosmosis through an Infinite Cylindrical Pore.** We assume throughout this article that the perturbation of the equilibrium charge cloud by the applied electric field and by fluid motion is negligibly small. The force acting on the ions in the charge cloud due to the applied electric field $-\nabla\chi$ is therefore $-\rho_0\nabla\chi$.

The equilibrium potential within an infinite cylindrical pore is

$$\phi_0 = \zeta_c\frac{I_0(\kappa r)}{I_0(\kappa a)} = \frac{\sigma_c}{\epsilon\kappa}\frac{I_0(\kappa r)}{I_1(\kappa a)} \tag{15}$$

In the absence of any end effects, if the electric field $E_0 = -\epsilon_2/h$ is applied along the length of the cylindrical pore, then the fluid velocity is[15]

$$u = \frac{\epsilon\phi_2}{\mu h}(\zeta_c - \phi_0) \tag{16}$$

and the total electroosmotic volumetric flow rate is[2]

$$Q_{ce} = \frac{2\pi\sigma_c a^3}{\mu h}\left[\frac{1}{2\kappa a}\frac{I_0(\kappa a)}{I_1(\kappa a)} - \frac{1}{(\kappa a)^2}\right]\phi_2 = H_c\phi_2 \tag{17}$$

where the electroosmotic coefficient

$$H_c = Q_{ce}/\phi_2 \sim \frac{\pi\sigma_c a^2}{\mu h\kappa} = \frac{\pi a^2\zeta_c}{\mu h\epsilon}, \quad a\kappa \gg 1 \tag{18a}$$

$$\sim\frac{\pi\sigma_c a^3}{4\mu h}, \quad a\kappa \ll 1. \tag{18b}$$

The total current through the cylindrical pore is $I_c$ (11), so the ratio between volume flux and current is

$$K_c = -Q_{ce}/I_c = H_c R_c \sim \frac{\sigma_c}{\mu\kappa\sum} = \frac{\zeta_c}{\mu \in \sum}, \quad a\kappa \gg 1 \tag{19a}$$

$$\sim\frac{\sigma_c a}{4\mu\sum}, \quad a\kappa \ll 1 \tag{19b}$$

**2.4. Electroosmosis through a Membrane ($h$ = 0).** It was shown by Mao et al.[1] that if the equilibrium charge density is $\rho_0$, then the imposed electric field is $\mathbf{E} = -\nabla\chi$ and the fluid velocity generated by a pressure difference $p_1$ across a pore (of arbitrary geometry) is

$$\mathbf{u} = p_1\mathbf{G} \tag{20}$$

then the reciprocal theorem[16] for Stokes flows can be used to show that electroosmotically generated volumetric flow rate through the pore is

$$Q = -\int_V \rho_0\mathbf{G}.\ \nabla\chi\ \mathrm{d}V \tag{21}$$

where the integral is over all the fluid.

The fluid velocity generated by the pressure difference $p_1$ across a circular hole in a membrane of zero thickness is

$$\mathbf{u} = p_1\mathbf{G}^m \tag{22}$$

An explicit expression for $\mathbf{G}^m(r,z)$ is available,[1,16] and the potential $\chi$ is given by eq 6. The charge density in the equilibrium charge cloud around a membrane of zero thickness is[1]


dx.doi.org/10.1021/la502349g | Langmuir XXXX, XXX, XXX−XXX

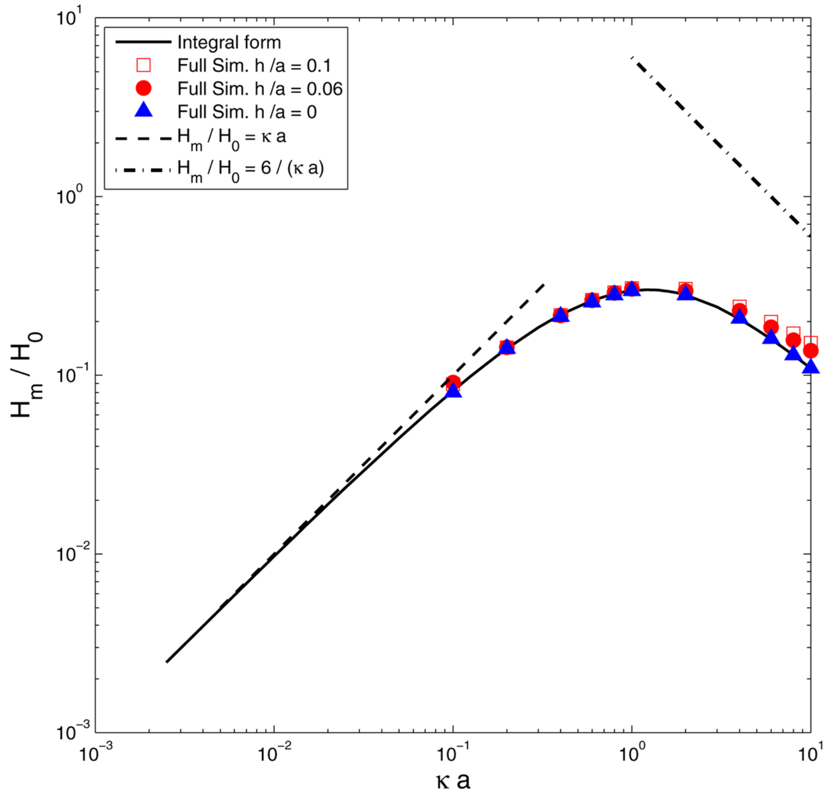


**Figure 3.** Electroosmotic coefficient $H_m$, scaled by $H_0$ (26), for a membrane of thickness $h = 0$, as a function of $a\kappa$. Solid line, analytic result (21); dashed line, asymptote (25) for $a\kappa \ll 1$; triangles, full PNP numerical computation ($h = 0$). The dot−dashed line shows $H_m/H_0 = 6/(a\kappa)$ with the expected slope for large $a\kappa$. Squares and circles show electroosmotic coefficients $H/H_0$ for nonzero membrane thickness $h > 0$, computed by numerical integration of the full PNP equations: solid circles, $h/a = 0.06$; open squares, $h/a = 0.1$.

$$\rho_0 = \sigma_m \kappa^2 a \left[ \int_0^\infty \frac{J_1(as) J_0(rs)}{(\kappa^2 + s^2)^{1/2}} e^{-(\kappa^2+s^2)^{1/2} z} \, ds - \frac{e^{-\kappa z}}{\kappa a} \right] \tag{23}$$

which consists of the charge density adjacent to a uniform charged surface, from which has been subtracted the charge density around a uniformly charged disk. The integral (21) can be evaluated numerically,[1] and the electroosmotic flow rate through a hole in a membrane of zero thickness can be expressed in the form

$$Q_{me} = H_m \phi_1 \tag{24}$$

where

$$H_m \sim a\kappa H_0, \quad a\kappa \ll 1 \tag{25}$$

with

$$H_0 = \frac{a^2 \sigma_m}{3\mu} \tag{26}$$

The ratio of the electroosmotic volume flux $Q_{me}$ to the electrical current $I_m$ is

$$Q_{me}/I_m = -K_m \tag{27}$$

where

$$K_m = H_m R_m \sim \frac{a\kappa}{2} K_0, \quad a\kappa \ll 1 \tag{28}$$

with

$$K_0 = \frac{a\sigma}{3\Sigma\mu} \tag{29}$$

Figure 3 shows a log−log plot of results for $H_m/H_0$ obtained by Mao et al.[1] The continuous line shows the analytic result (21) obtained via the reciprocal theorem, and the asymptote (25) for $a\kappa \ll 1$ is indicated.

The membrane has zero thickness, so there is always a region near the edge of the pore where the Debye length $\kappa^{-1}$ cannot be considered small compared with $h$; Smoluchowski's analysis for thin charge clouds, which would predict $H = 6H_0/(a\kappa)$ if $\zeta_m$ took the uniform value $\epsilon\kappa\sigma_m$, therefore, cannot automatically be invoked when $a\kappa \gg 1$. However, if we set up a local coordinate $s$ indicating distance from the edge of the pore, then both the electric potential $\chi$ (6) and the fluid velocity $\mathbf{G}^m$ (22) vary as $s^{1/2}$ when $s \ll a$ (i.e., near the pore edge). The charge cloud density $\rho_0$ decays over a length scale $\kappa^{-1}$, and only counterions of membrane surface charge within a distance $\kappa^{-1}$ from the edge contribute to $\rho_0$ within the hole. The contribution of the edge to the integral (21) is therefore $O((a\kappa)^{-1})$, as was similarly found for the electrophoretic velocity of a charged disk.[17] We therefore expect $H_m \sim H_0/(a\kappa)$ when $a\kappa \gg 1$. The data in Figure 3 do not extend to sufficiently high values of $a\kappa$ to allow us to estimate the asymptote with any accuracy, and for the figure, we simply indicate the line $H_m/H_0 = 6/(a\kappa)$ suggested by the Smoluchowski analysis. A similar reduction in the broadside electrophoretic velocity of a disk below the value predicted by Smoluchowski was noted by Sherwood and Stone.[17] Individual points in Figure 3 indicate results obtained from full numerical solutions of the Poisson−Nernst−Planck equations in a symmetric electrolyte at low applied potential


dx.doi.org/10.1021/la502349g | Langmuir XXXX, XXX, XXX−XXX

and low surface charge. In the computations, the length of the reservoirs in the $z$ direction was equal to their radius $b$, with $b = \max(10a, 10\kappa^{-1})$. Other details of the computations are reported in section 3.

**2.5. Composite Electroosmotic Coefficient $H_{comp}$.** When $h > 0$, it is natural to suppose that the electric field outside the membrane pumps fluid toward the cylindrical pore at a rate

$$Q_{me} \approx H_m(\phi_1 - \phi_2) \tag{30}$$

and the electric field within the cylindrical pore pumps fluid through the pore at a rate

$$Q_{ce} \approx H_c\phi_2 \tag{31}$$

However, in general, $Q_{me}$ (30) and $Q_{ce}$ (31) differ, and a pressure $\pm p_2/2$ builds up at $z = \pm h/2$ (i.e., at the entrance and exit to the cylindrical pore) in order to ensure that the volumetric flow rate is continuous. We now determine this pressure $p_2$.

Consider a membrane of zero thickness ($h = 0$), with pressure $p = p_1/2$ (above the reference ambient pressure) at infinity on the side $z > 0$ and with $p = -p_1/2$ at infinity on the other side. The pressure within the hole in the membrane is

$$p = 0, \quad z = 0, r < a, h = 0 \tag{32}$$

The fluid velocity generated by the pressure difference $p_1$ across the membrane is $\mathbf{u} = p_1\mathbf{G}^m$ (22), and the corresponding volumetric flow rate is[16]

$$Q_{mh} = G_m p_1, \quad G_m = -\frac{a^3}{3\mu} \tag{33}$$

If $h > 0$, then we approximate the pressure field in the fluid in much the same way as we approximated the electrical potential within the fluid: we patch a linearly varying pressure $p(z)$ within the cylindrical pore to the pressure field outside a membrane of zero thickness, and we take the pressure over the two ends $z = \pm h/2$ of the cylindrical pore to be $\pm p_2/2$. Thus, the pressure within the pore is approximated as

$$p = \frac{p_2}{h}z, \quad r < a, |z| < h/2 \tag{34}$$

the fluid velocity within the pore is

$$\mathbf{u} = p_2\mathbf{G}^c \tag{35}$$

and the volumetric flow rate within the pore is

$$Q_{ch} = G_c p_2, \quad G_c = -\frac{\pi a^4}{8h\mu} \tag{36}$$

Outside the cylindrical pore, the fluid velocity is now assumed to be

$$\mathbf{u} = (p_1 - p_2)\mathbf{G}^m(r, z - h/2), \quad z > h/2 \tag{37}$$

with $u_r(r,z) = -u_r(r,-z)$ and $u_z(r,z) = u_z(r,-z)$. The volumetric flow rate outside the membrane is now

$$Q_{mh} = G_m(p_1 - p_2), \quad G_m = -\frac{a^3}{3\mu} \tag{38}$$

We have ensured that the pressure (but not the fluid velocity or the volumetric flow rate) is continuous across the ends $z = \pm h/2$ of the cylindrical pore.

When an electric field generates an electroosmotic velocity, the volumetric flow rates within the cylindrical pore and outside the membrane are identical if $p_2$ is such that $Q_{mh} + Q_{me} = Q_{ch} + Q_{ce}$, i.e., if

$$G_m(p_1 - p_2) + H_m(\phi_1 - \phi_2) = G_c p_2 + H_c\phi_2 \tag{39}$$

But the pressure at infinity is zero in the electroosmotic problem, so $p_1 = 0$, and $\phi_2$ is given by eq 13. Hence

$$p_2 = \frac{H_m R_m - H_c R_c}{(G_m + G_c)(R_m + R_c)}\phi_1 \tag{40}$$

and the total electroosmotic flow is

$$Q_E = Q_{me} + Q_{mh} = \frac{(G_m R_c H_c + G_c H_m R_m)}{(R_m + R_c)(G_m + G_c)}\phi_1 = H_{comp}\phi_1 \tag{41}$$

An alternative derivation of this approximate composite $H_{comp}$ (41) is given in the next section.

Inserting into eq 41 the various estimates for $G_m$ (38), $G_c$ (36), $R_m$ (8), and $R_c$ (11), we obtain

$$H_{comp} = \frac{\left(H_m + \frac{16h^2}{3\pi^2 a^2}H_c\right)}{\left(1 + \frac{2h}{\pi a}\right)\left(1 + \frac{8h}{3\pi a}\right)} \tag{42}$$

For small $h/a$, the approximate composite $H_{comp}$ is larger than $H_m$ if

$$\frac{H_c}{H_m} > \frac{7\pi a}{8h} \tag{43}$$

Experimental arrangements sometimes involve measurements at fixed current, and a coefficient $K_{comp}$ that gives the electroosmotic flux per unit current is therefore useful. This quantity may be obtained readily from eqs 11, 13, and 41

$$K_{comp} = -\frac{Q_E}{I_c} = \frac{(G_m K_c + G_c K_m)}{(G_m + G_c)} = \frac{\left(K_m + \frac{8h}{3\pi a}K_c\right)}{\left(1 + \frac{8h}{3\pi a}\right)} \tag{44}$$

which changes from $K_m$ when $h = 0$ to $K_c$ when $h \gg a$.

**2.6. Composite Electroosmotic Coefficient $H_{comp}$ Derived via the Reciprocal Theorem.** We now show that approximations to the electric potential $\chi$ and pressure-driven velocity $\mathbf{G}$ within a pore of nonzero length $h > 0$, when inserted into the integral expression (21) for the electroosmotic volume flux, lead to an approximate electroosmotic coefficient identical to $H_{comp}$ (42) obtained in the previous section.

We have already shown that we may approximate the electric potential by a composite potential (9 and 10) of the form

$$\chi = \left(\frac{z}{h}\right)\frac{R_c\phi_1}{R_m + R_c}, \quad |z| < h/2 \tag{45a}$$

$$= \frac{R_c\phi_1}{2(R_m + R_c)} + \frac{R_m\phi_1}{(R_m + R_c)}\tilde{\chi}_m(r, z - h/2), \quad z > h/2 \tag{45b}$$

$$= \chi(r, -z), z < 0 \tag{45c}$$

We now create a similar approximation for the fluid velocity for flow through a membrane of thickness $h$ subjected only to a pressure drop $p_1$ but no applied potential drop. We suppose

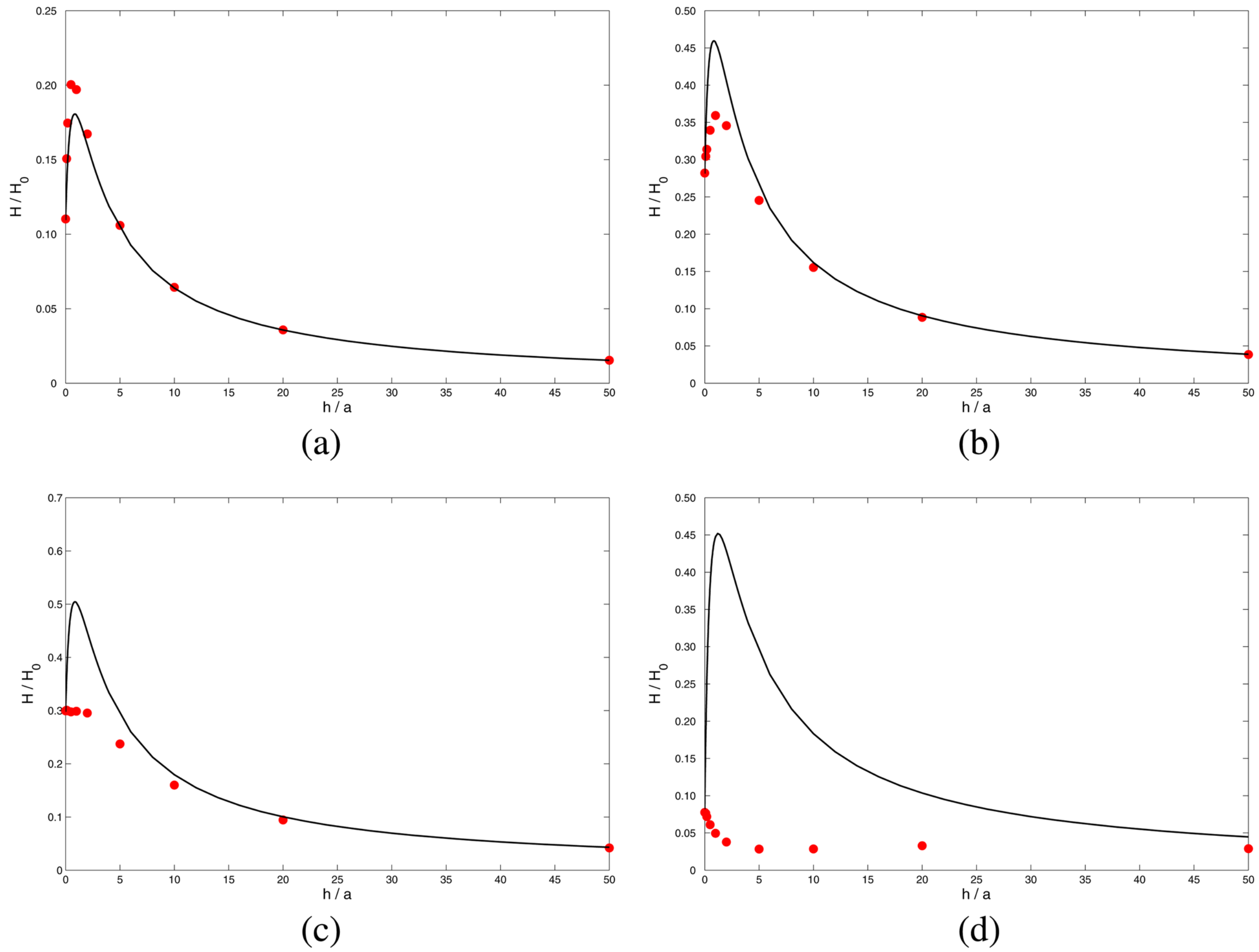


**Figure 4.** Electroosmotic coefficient $H$ scaled by $H_0$ (26) for $\sigma_m = \sigma_c$, as a function of $h/a$, for (a) $a\kappa = 10$, (b) $a\kappa = 2$, (c) $a\kappa = 1$, and (d) $a\kappa = 0.1$. Solid line, $H_{comp}$ (42); solid circles, full PNP numerical computation.

that in $z > h/2$ the fluid velocity is given by eq 37, corresponding to flow outside a membrane of zero thickness, and that within the cylindrical pore the fluid velocity is given by eq 35. Continuity of the volumetric flow rates 36 and 38 at the entrance to the cylindrical pore requires that the pressure $\pm p_2/2$ at the two ends of the pore satisfies

$$G_c p_2 = G_m(p_1 - p_2) \tag{46}$$

so that

$$p_2 = \frac{G_m p_1}{G_c + G_m} \tag{47}$$

Hence, our approximation to the fluid velocity is $\mathbf{u} = \mathbf{G}p_1$, with

$$\mathbf{G} = \frac{G_m}{G_c + G_m}\mathbf{G}^c(r, z), \qquad |z| < h/2 \tag{48a}$$

$$= \frac{G_c}{G_c + G_m}\mathbf{G}^m(r, z - h/2), \qquad z > h/2 \tag{48b}$$

The (small) errors involved in this approximation are discussed by Dagan et al.[18]

We now use approximations 45 and 48 in integral 21 in order to compute the electroosmotic volumetric flow rate. But the integration splits naturally into an integral over the cylindrical pore and an integral over the regions outside the membrane. The integral over the cylindrical pore is exactly the integral required to determine the electroosmotic flow rate $H_c$ (17) in a cylinder, and the integral outside the membrane is exactly that required to determine $H_m$ (24). Hence, the integral yields the composite electroosmotic flow rate

$$H_{comp} = \frac{G_c R_m H_m}{(G_c + G_m)(R_m + R_c)} + \frac{G_m R_c H_c}{(G_c + G_m)(R_m + R_c)} = \frac{G_c R_m H_m + G_m R_c H_c}{(G_c + G_m)(R_m + R_c)} \tag{49}$$

identical to 41, obtained in section 2.5 by elementary methods.

**2.7. Predictions of the Composite Electroosmotic Coefficient.** Figure 4 shows $H_{comp}$ (42) as a function of $h/a$ for four different values of $a\kappa$, with $\sigma_m = \sigma_c$. Also shown are the results of full numerical computations based on the Poisson−Nernst−Planck equations[1] and described in section 3. The coefficient $H_c$ (17) is proportional to $h^{-1}$ and is very large when the pore length $h$ is small, leading to a large electroosmotic coefficient $H_{comp}$. The action of the electric field acting on charge confined within the cylindrical pore is much more efficient at creating fluid motion than is the weaker electric field acting on charge outside the pore. We see that for $a\kappa \geq 1$ the approximate analysis captures the main features of the full numerical results, and it is clear from 42 that it also has the correct limits as $h/a \to 0$ and $h/a \to \infty$. However, it is also

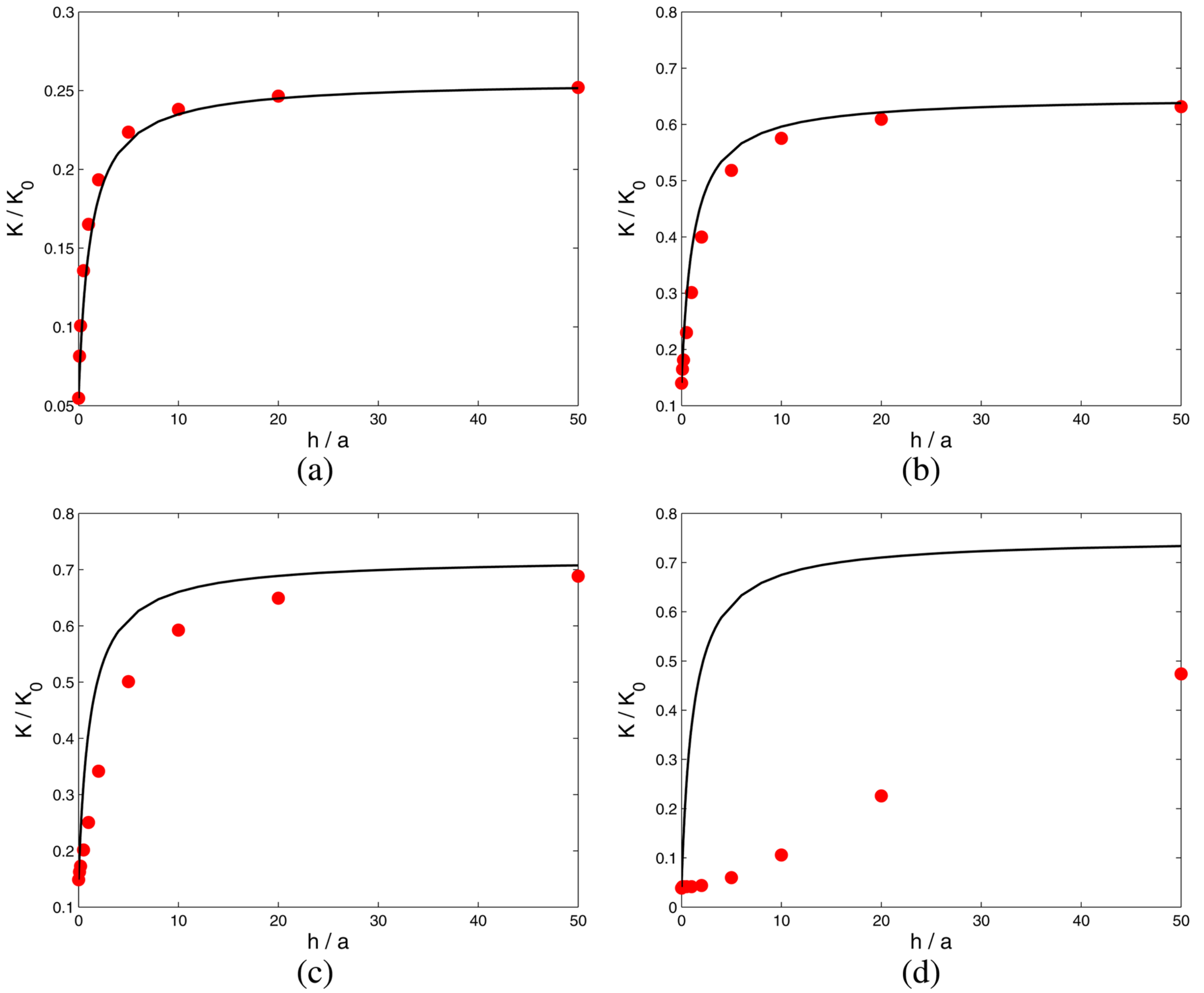


**Figure 5.** Results of Figure 4, presented in terms of the electroosmotic coefficient $K = HR_{tot}$ scaled by $K_0$ (29) for $\sigma_m = \sigma_c$, as a function of $h/a$, for (a) $a\kappa = 10$, (b) $a\kappa = 2$, (c) $a\kappa = 1$, and (d) $a\kappa = 0.1$. Solid line, $K_{comp}$ (44); solid circles, full PNP numerical computation.

evident from Figure 4d that the theory is unsatisfactory when $a\kappa \ll 1$.

The results of Figure 4 are presented in terms of the coefficient $K_{comp}$ (44) in Figure 5. Both $K_{comp}$ and the full numerical results now increase monotonically with $h$, with a final end point $K_{comp} = K_c$ that is independent of $h$ when $h \gg a$. Figure 5, like Figure 4, shows that the theory leading to $K_{comp}$ is inadequate when $a\kappa \ll 1$. We discuss this limit in section 4, where we shall show that when $a\kappa \ll 1$ some of the charge cloud of ions that neutralizes the surface charge on the cylindrical wall of the pore spills out of the ends of the pore, where it is less effective at generating electroosmotic flow. The scenario is shown schematically in Figure 6.

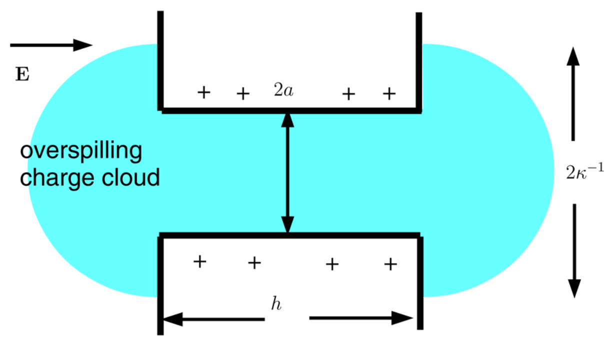


**Figure 6.** When the Debye length $\kappa^{-1}$ is large compared with the pore radius $a$, the cloud of counterions associated with the charged cylindrical wall of the pore spills out of the ends of the pore.

## 3. NUMERICAL SIMULATION

The time-independent PNP–Stokes equations governing the electrical potential $\phi$, the ionic number density of the $i$th ionic species $n^i$ ($i = 1, ..., N$), the fluid velocity $\mathbf{u}$ and fluid pressure $p$ are

$$\epsilon\nabla^2\phi + \sum_{i=1}^{N} z_i e n^i = 0 \tag{50}$$

$$\nabla\cdot[n^i\mathbf{u} - \omega^i(kT\nabla n^i + ez_i n^i\nabla\phi)] = 0 \tag{51}$$

$$-\nabla p + \mu\nabla^2\mathbf{u} - \nabla\phi \sum_{i=1}^{N} z_i e n^i = 0 \tag{52}$$

$$\nabla\cdot\mathbf{u} = 0 \tag{53}$$

where $z_i$ is the valence of the $i$th ionic species and $\omega^i$ is its mobility. Here, we restrict our attention to the case $N = 2$, with $z_1 = -z_2 = 1$.

We used a finite volume numerical scheme to solve the system of coupled eqs 50−53 in the axisymmetric geometry depicted in Figure 1. Thus, we considered a cylindrical pore of radius $a$ and length $h$ connecting two large cylindrical reservoirs of radius $b$. The lengths of AB and EF in our simulation were also taken to be $b$, which was kept much larger than either $a$ or the Debye length $\kappa^{-1}$ so that the reservoirs were effectively infinite.

**3.1. Boundary Conditions.** At A and F, the two ends of the reservoirs, ion concentrations were set equal to the concentration in the bulk electrolyte (i.e., $n^i = n^i_\infty$); a potential difference $\Delta V$ was applied across the system by setting $\phi$ to $\pm\Delta V/2$, respectively, at A and F, where the pressures were set equal to the bulk pressure, $p = p_\infty$. At AB and EF, the side walls of the cylindrical reservoir, the radial component of the electric field, ionic flux, and velocity were all set to zero, as was the tangential shear stress, in order to minimize the effect of these boundaries. The last condition was imposed as the cylindrical reservoirs merely represent a convenient computational domain; the walls of the real physical reservoir are far enough away from the pore to be essentially irrelevant. At the membrane and pore surfaces, BC, CD, and DE, a no-flux condition was used for 51, and a no-slip condition was used for the flow. At solid−fluid interfaces (with unit normal $\hat{n}$), the electric potential is continuous, but the normal component of the electric field undergoes a jump, with $[\epsilon\mathbf{E}\cdot\hat{n}] = \sigma_m$ at BC and DE and $[\epsilon\mathbf{E}\cdot\hat{n}] = \sigma_c$ at CD.

An electrohydrodynamic solver was implemented to solve the system described above using the OpenFOAM CFD library,[20] a C++ library designed for computational mechanics. A structured mesh was constructed by means of the polyMesh meshing tool within OpenFOAM. The grid was refined near the membrane and pore surfaces to resolve the Debye layer. Grid independence was checked in all cases by refining the grid and verifying that the solution did not change within specified tolerances.

For the finite volume discretization of the governing equations, central differences were used for all diffusive terms in 51 and viscous terms in 52. A second-order upwind scheme was used for the convective terms in 51. The discretized linear system was solved using a preconditioned conjugate gradient solver if the matrix was symmetric or a preconditioned biconjugate gradient solver if the matrix was asymmetric.[21]

An iterative scheme was used to solve the PNP−Stokes equations. Initially, the flow velocity was set to zero. Equations 50 and 51 were then solved sequentially in a loop with under-relaxation (to ensure stability of the nonlinear PNP system) until the absolute residual was smaller than a specified tolerance, in our case, $10^{-6}$. The electric force density $-\nabla\phi\sum_i z_i e n^i$ was then obtained from this solution and used as an explicit external forcing in the solution of the incompressible Stokes flow problem, 52 and 53, solved by means of the SIMPLE algorithm. The flow field so computed was then substituted into 51, and the PNP equations were solved again using the updated flow field. An outer loop was constructed to iterate over the PNP loop and Stokes flow module until the solution changed negligibly between two outer iterations.

Our main object of interest is the volumetric flux, $Q$. This was obtained by numerically integrating the axial velocity over the plane $z = 0$. At the low voltages employed, the linear relation found between $Q$ and $\Delta V$ leads to the electroosmotic coefficient $H = Q/\Delta V$, shown as discrete points in Figures 3−5 and 7. The amount of charge within the pore was determined by numerical integration and used to obtain the quantities $h_{\text{lost}}$ and $h_{\text{gained}}$ reported in Table 1.

## 4. CHARGE OVERSPILL FROM THE ENDS OF THE PORE, $A\kappa \ll 1$

**4.1. Overspill of Charge from the End of a Semi-Infinite Pore.** We consider a cylindrical pore of radius $a$, with surface charge density $\sigma_c$. When the Debye length $\kappa^{-1} \gg a$, the equilibrium potential $\phi_0$ (15) in an infinitely long cylinder can be expanded as

$$\phi_0 = \phi_a\left(1 + \frac{(\kappa r)^2}{4} + \cdots\right) \tag{54}$$

where

$$\epsilon_a = \frac{\sigma_c}{\epsilon\kappa I_1(\kappa a)} \approx \frac{2\sigma_c}{\epsilon\kappa(\kappa a)} \tag{55}$$

Thus, the equilibrium potential $\phi_0$ and charge density $\rho_0 = -\epsilon\kappa^2\phi_0$ within the charge cloud vary little over the cross-section of the pore. On the other hand, if the cylinder is not infinitely long and uniform, $\phi_0$ and $\rho_0$ vary in the axial ($z$) direction with a length scale $\kappa^{-1}$. We can therefore consider the equilibrium potential $\phi_0$ within the cylindrical pore to be a function only of $z$.[19]

We first consider a semi-infinite, charged cylindrical pore going from $z = 0$ to $z = \infty$. The equilibrium potential $\phi_0$ satisfies a one-dimensional Poisson−Boltzmann equation

$$\frac{\mathrm{d}^2\phi_0}{\mathrm{d}z^2} = -\kappa^2\phi_0 \tag{56}$$

The solution that tends to the uniform potential $\phi_a$ within the pore as $z \to \infty$ far from the pore end at $z = 0$, is

$$\phi_0 = \phi_a - A\exp(-\kappa z) \tag{57}$$

for some unknown constant $A$. The charge density within the charge cloud inside the pore is $-\epsilon\kappa^2\phi_0$, and when the cylindrical pore is infinite (and hence uniform) the charge per unit length in the charge cloud is $-\pi a^2\epsilon\kappa^2\phi_a = -2\pi\sigma_c a$, equal and opposite to the charge per unit length on the pore walls. When the pore is semi-infinite, with a nonuniform charge cloud (57), the total charge that is lost from within the pore is

$$q_{\text{lost}} = -\pi a^2\epsilon\kappa^2\int_0^\infty(\phi_a - \phi_0)\,\mathrm{d}z = -\pi a^2\kappa\epsilon A \tag{58}$$

At the end of the pore (z = 0), the potential is $\phi = \phi_a - A$.

In $z < 0$, the charge cloud is no longer confined by the walls of the cylindrical pore and spreads out radially: it is no longer possible to assume that $\phi_0$ is a function of $z$ alone. We therefore need to solve the linearized Poisson−Boltzmann equation in the half-space $z < 0$, with $\phi_0 = \phi_a - A$ over the region $z = 0$, $r < a$ and $\partial\phi_0/\partial z = 0$ on $z = 0$, $r > a$. At large distances from the end of the pore, the potential decays as $\exp(-\kappa R)/R$, where $R =$

$(z^2 + r^2)^{1/2}$ is a spherical polar coordinate, but in the important region $R = O(a)$, the potential can be approximated by the electrostatic potential corresponding to a solution of the Laplace equation (i.e., $\kappa = 0$). Hence, from 6,

$$\phi_0 = (\phi_a - A)\frac{2}{\pi}\tan^{-1}\left(\frac{1}{\sinh \xi}\right) \tag{59}$$

To relate the potential (59) to the amount of charge in the overspilling charge cloud (in $z < 0$), we note that the charge on one side of a charged disk at uniform potential $(\phi_a - A)$ in unbounded space is $q = 4a\epsilon(\phi_a - A)$. Alternatively, one can argue that far from the plane $z = 0$, the spherical distance $R \approx a \cosh \xi$, so that the potential (59) is approximately

$$\phi_0 \approx (\phi_a - A)\frac{2a}{\pi R} \tag{60}$$

In a spherically symmetric geometry this field corresponds to the far field around a point charge of magnitude $8a\epsilon(\phi_a - A)$, and the total surface charge on one side of the disk is $q = 4a\epsilon(\phi_a - A)$, in agreement with the charge obtained by considering the capacitance of the disk. The charge in the overspill charge cloud in $z < 0$ is equal and opposite to $q$ and is therefore

$$q_{\text{overspill}} = -4a\epsilon\phi_0(z = 0) = -4a\epsilon(\phi_a - A) \tag{61}$$

But the total charge (61) in the overspill outside the end of the pore must be equal to the charge (58) that has been lost from within the pore. Hence

$$4a\epsilon(\phi_a - A) = \pi a^2\kappa\epsilon A \tag{62}$$

so that

$$A = \frac{\phi_a}{1 + \pi a\kappa/4} \tag{63}$$

and the potential at the end of the pore is

$$\phi_a - A = \frac{\phi_a}{1 + 4/(\pi a\kappa)} \tag{64}$$

The charge that has been lost from the end of the pore is equivalent to the charge usually found in a pore of length

$$h_{\text{lost}} = -\frac{q_{\text{overspill}}}{2\pi a\sigma_c} = \frac{4}{4\kappa + \pi a\kappa^2} \tag{65}$$

The loss of charge implies that the combined charge cloud and wall surface charge over a cross-section of constant $z$ are no longer electrically neutral, as pointed out by Baldessari and Santiago.[4,6,7]

**4.2. Overspill from the Two Ends of a Finite Pore.** We can now perform the same analysis for a pore that occupies the region $-h/2 < z < h/2$. The equilibrium potential within the pore has the form

$$\phi_0 = C - B\cosh(\kappa z) \tag{66}$$

where we have chosen the solution that is symmetric about the center of the pore at $z = 0$. The charge that has been lost from within the pore is

$$\begin{aligned} q_{\text{lost}} &= -\epsilon\kappa^2\pi a^2\left(\int_{-h/2}^{h/2}(\phi_0 - \phi_a)\,dz\right) \\ &= \epsilon\pi a^2\kappa^2\left[\frac{2B}{\kappa}\sinh\left(\frac{\kappa h}{2}\right) + (\phi_a - C)h\right] \end{aligned} \tag{67}$$

The total flux of electric field through the two ends of the pore is

$$2\pi a^2\frac{\partial\phi_0}{\partial z}\bigg|_{z=h/2} = -2\pi a^2\kappa B\sinh\left(\frac{\kappa h}{2}\right) \tag{68}$$

Comparing 67 and 68, we conclude that $C = \phi_a$. The potential over the ends of the pore is

$$\phi_0(h/2) = \phi_0(-h/2) = \phi_a - B\cosh(\kappa h/2) \tag{69}$$

The total charge in the two overspill charge clouds is therefore, by 61,

$$q_{\text{overspill}} = -8a\epsilon\left[\phi_a - B\cosh\left(\frac{\kappa h}{2}\right)\right] \tag{70}$$

and this must be equal to the charge (67) lost from within the pore. Hence

$$B = \frac{4\phi_a}{4\cosh(\kappa h/2) + \pi a\kappa\sinh(\kappa h/2)} \tag{71}$$

and

$$\phi_a - B\cosh\left(\frac{\kappa h}{2}\right) = \frac{\phi_a\pi a\kappa\sinh(\kappa h/2)}{4\cosh(\kappa h/2) + \pi a\kappa\sinh(\kappa h/2)} \tag{72}$$

The total charge that has been lost (from the two ends) is equivalent to a total lost length

$$h_{\text{lost}} = -\frac{q_{\text{overspill}}}{2\pi a\sigma_c} = \frac{8\sinh(\kappa h/2)}{4\kappa\cosh(\kappa h/2) + \pi a\kappa^2\sinh(\kappa h/2)} \tag{73}$$

$$\sim \frac{8}{4\kappa + \pi a\kappa^2}, \quad \kappa h \gg 1 \tag{74}$$

$$\sim \frac{4h}{4 + \pi a h\kappa^2/2}, \quad \kappa h \ll 1. \tag{75}$$

We see from eqs 65 and 74 that when $\kappa h \gg 1$ the lost charge is twice that lost from a single end of a pore. We also note that $h - h_{\text{lost}} > 0$, and that when the pore is short $(\kappa h \ll 1)$ the amount of charge remaining within the cloud within the pore is proportional to

$$h - h_{\text{lost}} \sim \frac{\pi a\kappa^2 h^2}{8 + \pi a h\kappa^2}, \quad \kappa h \ll 1 \tag{76}$$

**4.3. Overspill from the Membrane Surface into the Pore.** If the cylindrical pore itself is uncharged, but the membrane surfaces are charged, ions from the charge cloud adjacent to the membrane surface are able to move into the ends of the pore.

If the membrane has zero thickness, then the charge density $\rho_0$ in the equilibrium charge cloud is given by 23, and both $\rho_0$ and the potential $\phi_0 = -\rho_0/(\epsilon\kappa^2)$ vary over the area of the pore. Nevertheless, we may work out the mean potential over the circular pore

$$\bar{\phi}_0 = -\frac{1}{\epsilon\kappa^2\pi a^2}\int_0^a 2\pi r\rho_0\,\mathrm{d}r = \frac{2\sigma_\mathrm{m}}{\epsilon a}\left[\frac{a}{2\kappa} - \int_0^\infty \frac{aJ_1(as)J_1(as)}{s(\kappa^2+s^2)^{1/2}}\,\mathrm{d}s\right] \tag{77}$$

where, when $a\kappa \ll 1$

$$\int_0^\infty \frac{aJ_1(as)J_1(as)}{s(\kappa^2+s^2)^{1/2}}\,\mathrm{d}s \approx a^2\int_0^\infty \frac{J_1(t)J_1(t)}{t^2}\,\mathrm{d}t = \frac{4a^2}{3\pi} \tag{78}$$

Thus, when the membrane has zero thickness (and there is no cylindrical pore into which ions can escape) the absence of surface charge over the area of the pore changes the average potential over the opening from the value $\phi_0 = \sigma_\mathrm{m}/(\epsilon\kappa)$ due to a uniformly charged surface to $\beta\sigma_\mathrm{m}/(\epsilon\kappa)$, where

$$\beta \approx 1 - \frac{8a\kappa}{3\pi}, \qquad a\kappa \ll 1 \tag{79}$$

We now consider the charge that leaks into a pore of length $h > 0$ from the charge clouds on either side of the membrane. We suppose that the potential on the planes $z = \pm h/2$ is perturbed by an amount $D$ and becomes

$$\phi_0 = \frac{\beta\sigma_\mathrm{m}}{\epsilon\kappa} + D, \qquad z = \pm h/2 \tag{80}$$

Within the pore, the potential obeys the one-dimensional Poisson–Boltzmann equation (52), with solution

$$\phi_0 = \left(\frac{\beta\sigma_\mathrm{m}}{\epsilon\kappa} + D\right)\frac{\cosh(\kappa z)}{\cosh(\kappa h/2)} \tag{81}$$

and the additional charge within the pore is

$$q_\mathrm{in} - \epsilon\kappa^2\pi a^2\int_{-h/2}^{h/2}\phi_0\,\mathrm{d}z = -\pi a^2(\beta\sigma_\mathrm{m} + D\epsilon\kappa)\frac{2\sinh(\kappa h/2)}{\cosh(\kappa h/2)} \tag{82}$$

Outside the pore, the perturbed potential (80) is associated with a total additional charge (61)

$$q_\mathrm{out} = -8a\epsilon D \tag{83}$$

on the two sides of the membrane. But the total change in charge caused by this redistribution must be zero, i.e., $q_\mathrm{in} + q_\mathrm{out} = 0$. Hence

$$\pi a^2(\beta\sigma_\mathrm{m} + D\epsilon\kappa)\frac{2\sinh(\kappa h/2)}{\cosh(\kappa h/2)} + 8a\epsilon D = 0 \tag{84}$$

i.e.

$$D = -\frac{\pi a\beta\sigma_\mathrm{m}\sinh(\kappa h/2)}{[4\cosh(\kappa h/2) + \pi a\kappa\sinh(\kappa h/2)]\epsilon} \tag{85}$$

The total charge $q_\mathrm{in} = -q_\mathrm{out}$ (83) that leaks into the pore at the two ends corresponds to the charge inside a uniformly charged cylinder with surface charge density $\sigma_\mathrm{m}$, of length

$$h_\mathrm{gained} = -\frac{8a\epsilon D}{2\pi a\sigma_\mathrm{m}} = \frac{4a\beta\sinh(\kappa h/2)}{4\cosh(\kappa h/2) + \pi a\kappa\sinh(\kappa h/2)} = \frac{a\kappa\beta}{2}h_\mathrm{lost} \tag{86}$$

$$\sim \frac{a\kappa\beta h}{2}, \qquad \kappa h \ll 1 \tag{87}$$

$$\sim \frac{a\beta}{2 + \pi a\kappa}, \qquad \kappa h \gg 1 \tag{88}$$

Thus, $h_\mathrm{gained}$ (86) is smaller than $h_\mathrm{lost}$ (73) by a factor $a\kappa\beta/2$. We can compare predictions 73 and 86 against results obtained from full numerical solution of the nonlinear Poisson–Boltzmann equation with either $\sigma_\mathrm{m} = 0$ and $ae\sigma_\mathrm{c}/(\epsilon kT) = a\kappa e\zeta_\mathrm{c}/(kT) = 0.00273$ or $\sigma_\mathrm{c} = 0$ and $ae\sigma_\mathrm{m}/(\epsilon kT) = 0.00273$: results for $a\kappa = 0.1$ are given in Table 1. We see that there is excellent agreement between the numerical computations and the analysis presented above.

**Table 1. Charge Lost from the Ends of a Charged Pore When the Membrane Charge Density $\sigma_\mathrm{m} = 0$[a] and the Charge Gained Inside an Uncharged Pore ($\sigma_c = 0$) from the Charge Cloud Adjacent to the Charged Membrane Surface[b,c]**

| | | $h_\mathrm{lost}/a$ | | $h_\mathrm{gained}/a$ | |
|---|---|---|---|---|---|
| $h/a$ | $h\kappa$ | theory (69) | numerical | theory (82) | numerical |
| 10.0 | 1.0 | 8.9186 | 8.9249 | 0.4081 | 0.4119 |
| 1.0 | 0.1 | 0.9953 | 0.9954 | 0.0455 | 0.0459 |
| 0.1 | 0.01 | 0.1000 | 0.1000 | 0.0046 | 0.0046 |

[a]In terms of an equivalent pore length $h_\mathrm{lost}$ (73). [b]In terms of an equivalent pore length $h_\mathrm{gained}$ (86). [c]$a\kappa = 0.1$.

**4.4. Composite Electroosmotic Coefficient.** We first consider how the electroosmotic coefficients $H_\mathrm{c}$ and $H_\mathrm{m}$ are modified by the overspill of the charge cloud from inside the cylindrical pore to outside the membrane. If a uniform electric field of strength $E = -\phi_1/h$ is applied between the ends of the pore, then the Navier–Stokes equations for steady flow yield the axial velocity profile

$$u = \frac{a^2 - r^2}{4\mu}\left(\rho_0 E - \frac{\mathrm{d}p}{\mathrm{d}z}\right) \tag{89}$$

so that the volumetric flow rate is

$$Q = \frac{a^4\pi}{8\mu}\left(\rho_0 E - \frac{\mathrm{d}p}{\mathrm{d}z}\right) \tag{90}$$

But $Q$ is independent of $z$ (by incompressibility), and the pressure $p$ difference between the two ends of the capillary is zero. Hence, integrating 90 along the length $h$ of the cylindrical pore and noting that the total amount of charge in the charge cloud remaining within the pore is $2\pi a\sigma_\mathrm{c}(h - h_\mathrm{lost})$, we find

$$Q = \frac{a^4\pi E}{8h\mu}\int_{-h/2}^{h/2}\rho_0\,\mathrm{d}z = \frac{\pi a^3\sigma_\mathrm{c}(h - h_\mathrm{lost})\phi_1}{4h^2\mu} = H_\mathrm{c}\phi_1 \tag{91}$$

which may be compared to the result (18b) which ignores overspill. The charge cloud outside the pore is enhanced by the overspill and becomes (in $z > 0$)

$$\rho_0 = -\sigma_\mathrm{m}\kappa\exp(-\kappa z) - \frac{2\epsilon\kappa^2}{\pi}[\phi_a - B\cosh(\kappa h/2)]\tan^{-1}\left(\frac{1}{\sinh\xi}\right) \tag{92}$$

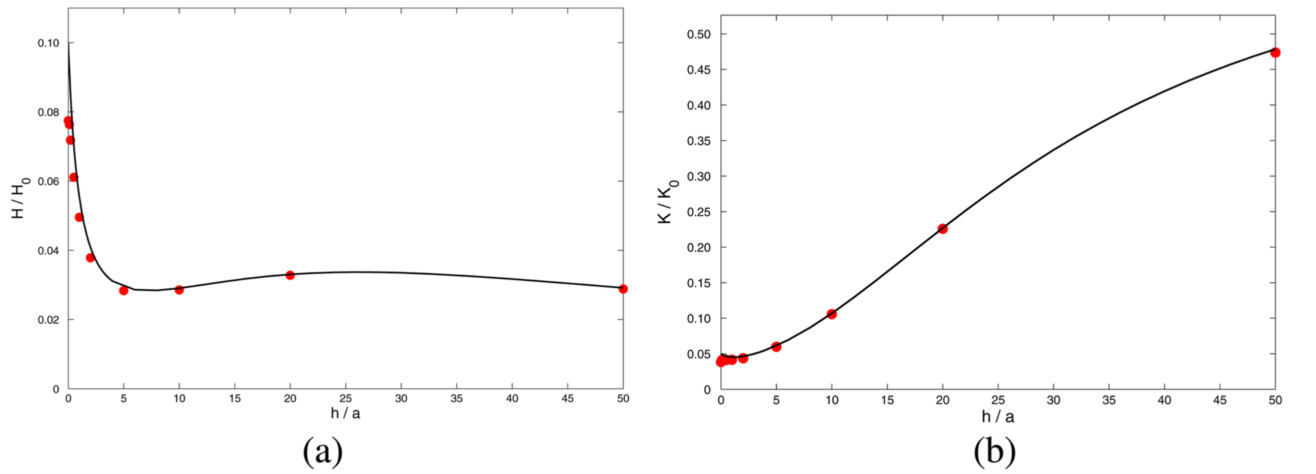


**Figure 7.** (a) Electroosmotic coefficient $H$ scaled by $H_0$ (26) for $\sigma_m = \sigma_c$, as a function of $h/a$, for $a\kappa = 0.1$, including the effect of overspilling charge clouds. Solid line, $H_{comp}$ (40), using $H_c$ given by 96 and $H_m$ given by 97; solid circles, full PNP numerical computation (cf. Figure 4d, in which overspill was neglected). (b) The same results, presented in terms of $K = R_{tot}H$ scaled by $K_0$ (29). Solid line, $K_{comp}$ (44), using $K_c = R_cH_c$ and $K_m = R_mH_m$; solid circles, full computation (cf. Figure 5d).

with the final term $[\phi_a - B\cosh(\kappa h/2)]$, corresponding to the overspill charge cloud (68), being approximately valid in a volume $O(a^3)$ around the pore, but invalid at large distance $O(\kappa^{-1})$ from the pore, where the exponential decay of the charge density is not captured by the solution (59) of the Laplace equation. The volumetric flow rate through a pore of zero thickness created by a potential difference $\phi_1$ is given by the integral (21) and was shown by Mao et al.[1] to be

$$\begin{aligned} Q &= \frac{2a^3\phi_1}{\pi\mu}\int_0^{\pi/2} d\eta \int_0^{\infty} \rho_0 \frac{\cos^2\eta\,\sin\eta}{\cosh\xi}\,d\xi \\ &= -\frac{a^3\kappa\sigma_m\phi_1}{3\mu} - \frac{4\epsilon\kappa^2a^3\phi_1}{\pi^2\mu}(\phi_a - B) \\ &\quad \int_0^{\pi/2}\cos^2\eta\,\sin\eta\,d\eta\int_0^{\infty}\tan^{-1}\left(\frac{1}{\sinh\xi}\right)\frac{d\xi}{\cosh\xi} \\ &= -\frac{a^3\kappa\sigma_m}{3\mu}\phi_1 - \frac{4\epsilon a^3\kappa^2}{3\pi^2\mu}\phi_1(\phi_a - B)I_3 \end{aligned} \tag{93}$$

where

$$\begin{aligned} I_3 &= \int_0^{\infty}\tan^{-1}\left(\frac{1}{\sinh\xi}\right)\frac{d\xi}{\cosh\xi} = \int_0^{\infty}\tan^{-1}x\frac{dx}{1+x^2} \\ &= \frac{\pi^2}{8} \end{aligned} \tag{94}$$

Hence, the electroosmotic flow rate $Q = H_m\phi_1$ due to the charge cloud outside the membrane is modified, and $H_m$ becomes

$$H_m = \frac{a^3\kappa}{3\mu}\left[\sigma_m + \frac{\pi\sinh(\kappa h/2)\sigma_c}{4\cosh(\kappa h/2) + \pi a\kappa\sinh(\kappa h/2)}\right] \tag{95}$$

If $\sigma_m$ is comparable to $\sigma_c$, then we saw in section 4.3 that the change in the charge within the pore due to the charge cloud outside the membrane entering the pore is $O(a\kappa)$ smaller than the loss of charge from the charge cloud within the pore to the regions outside the membrane. However, this contribution can be included with very little effort and becomes important in the limit $h \to 0$, when the gain (87) in charge within the pore from the outside surface charge density $\sigma_m$ is proportional to $h_{gained} \propto h$, whereas the charge cloud (due to $\sigma_c$ within the pore) remaining within the pore is proportional to $h - h_{lost} \propto h^2$, by 76. The electroosmotic coefficient $H_c$ for the cylindrical pore (91) becomes

$$H_c = \frac{\pi a^3\sigma_c(h - h_{lost} + h_{gained}\sigma_m/\sigma_c)}{4h^2\mu} \tag{96}$$

and the electroosmotic coefficient $H_m$ for the charge cloud outside the membrane (95) becomes

$$H_m = \frac{a^3\kappa}{3\mu}\left[\sigma_m + \frac{\pi\sinh(\kappa h/2)(\sigma_c - a\kappa\beta\sigma_m/2)}{4\cosh(\kappa h/2) + \pi a\kappa\sinh(\kappa h/2)}\right] \tag{97}$$

Now that $H_c$ (96) and $H_m$ (97) have been corrected for the effects of overspill in the two directions, they can be inserted into expression 42 for the composite electroosmotic coefficient $H_{comp}$. Results are shown in Figure 7a, together with full numerical solutions of the Poisson–Nernst–Planck equations. We see that the agreement between theory and computation is much better than when overspill is ignored (Figure 4d). Charge overspill or underspill causes the total charge of mobile ions within the pore to differ from what might be expected on the basis of net electroneutrality of the pore. Thus, the driving force is modified, leading to deviations from the calculated result that ignores such effects. The "lost length" $h_{lost}$ in 96 restores this effect. Figure 7b shows the results of Figure 7a expressed in terms of $K$, rather than $H$, and there is again good agreement between the theoretical $K_{comp}$ and full numerical results.

Note that when $h \ll \kappa^{-1}$ the effective length of the cylindrical pore $h - h_{lost} \approx \pi a\kappa^2h/2$, by 76. The approximation (96) for $H_c$ is therefore dominated by the term $h_{gained}$ and gives $H_c \sim \pi a^4\kappa\beta\sigma_m/(8h\mu)$, with $H_c/H_m \sim 3\pi a\beta/(8h)$. We conclude from 43 that $H_{comp}$ is a decreasing function of $h$ near $h = 0$, as seen in Figure 7a.

## 5. CONCLUDING REMARKS

The analysis presented here shows that it is possible to use simple analyses based on continuity of volumetric flow rate and electric current to estimate electroosmotic end effects in a charged cylindrical pore traversing a membrane of thickness $h > 0$. Note that we have made repeated use of the assumption that surface charge densities, and corresponding zeta potentials, are small. We have not only worked with the linearized Poisson–Boltzmann eq 2 but also used superposition to combine various contributions to the charge clouds due to overspill of the clouds from one region (inside/outside the pore) to the other. At high potentials, it would also be necessary to keep track of the fluxes of individual ion species, rather than simply ensuring that the total electrical current is continuous.[9]

The assumption of small potentials also justifies our neglect of other nonlinear electrokinetic effects such as induced charge electroosmosis (ICEO),[22,23] which can produce vortices in the vicinity of sharp corners[24] or near rapid constrictions in channels[25] when the permittivity of the solid $\epsilon_s > 0$. However, numerical solutions confirm the expectation that the flow rate is only weakly affected by such vortices, particularly under conditions of small potentials.[26]

In recent experiments[27−31] on nanopores, potential differences of $\Delta\phi \sim 0$−200 mV were applied across the pore. Here, we have assumed that $\Delta\phi \ll \zeta$, where $\zeta$ itself is assumed small in comparison with the thermal voltage $kT/e \sim 25$ mV. Thus, our results can only be expected to describe the initial linear part of the current−voltage and flow−voltage characteristics, even though numerical simulations seem to show[26] that this linear regime extends to applied voltages ~100 mV.

Finally, we point out that the correction factor $\beta$ (79) reminds us that the hole in the charged membrane removes a circular region of surface charge and reduces the equilibrium potential at the entrance to the pore. The introduction of $\beta < 1$ improved the agreement between theoretical and numerical results for $h_{\text{gained}}$ in Table 1. However, the analysis is not rigorous, since the equilibrium potential across the hole is not uniform. The $O(1 - \beta)$ correction to the equilibrium potential corresponds to an $O(1 - \beta)$ correction to the charge density $\rho_0$. If we use this in the integral expression (89) in order to determine a correction to the electroosmotic flow rate through a membrane of zero thickness, then the analysis suggests that the correction to the leading order result (25) for $a\kappa \ll 1$ should be $O((a\kappa)^2)$, whereas investigation of the difference (seen in Figure 3) between numerical results and the asymptote (25) indicates additional corrections $O((a\kappa)^2 \ln a\kappa)$.

## ■ AUTHOR INFORMATION

### Corresponding Author

*E-mail: jds60@cam.ac.uk.

### Notes

The authors declare no competing financial interest.

## ■ ACKNOWLEDGMENTS

J.D.S. thanks the Department of Applied Mathematics, University of Cambridge, and the Institut de Mécanique des Fluides de Toulouse, for hospitality. M.M. and S.G. acknowledge support from the NIH through grant no. 4R01HG004842.

## ■ REFERENCES

(1) Mao, M.; Sherwood, J. D.; Ghosal, S. Electroosmotic flow through a nanopore. *J. Fluid Mech.* **2014**, *749*, 167−183.
(2) Rice, C.L.; Whitehead, R. Electrokinetic flow in a narrow cylindrical capillary. *J. Phys. Chem.* **1965**, *69*, 4017−4024.
(3) Gross, R. J.; Osterle, J. F. Membrane transport characteristics of ultrafine capillaries. *J. Chem. Phys.* **1968**, *49*, 228−234.
(4) Baldessari, F. Electrokinetics in nanochannels. Part I. Electric double layer overlap and channel-to-well equilibrium. *J. Colloid Interface Sci.* **2008**, *325*, 526−538.
(5) Baldessari, F. Electrokinetics in nanochannels. Part II. Mobility dependence on ion density and ionic current measurements. *J. Colloid Interface Sci.* **2008**, *325*, 539−546.
(6) Baldessari, F.; Santiago, J. G. Corrigendum to "Electrokinetics in nanochannels. Part I. Electric double layer overlap and channel-to-well equilibrium". *J. Colloid Interface Sci.* **2009**, *331*, 549.
(7) Baldessari, F.; Santiago, J. G. Corrigendum to "Electrokinetics in nanochannels. Part II. Mobility dependence on ion density and ionic current measurements". *J. Colloid Interface Sci.* **2009**, *331*, 550.
(8) Henry, D. C. The cataphoresis of suspended particles. *Proc. R. Soc. London, Ser. A* **1931**, *133*, 106−129.
(9) Biscombe, C. J. C; Davidson, M. R.; Harvie, D. J. E. Electrokinetic flow in connected channels: a comparison of two circuit models. *Microfluid. Nanofluid.* **2012**, *13*, 481−490.
(10) Jin, M.; Sharma, M. M. A model for electrochemical and electrokinetic coupling in inhomogeneous porous media. *J. Colloid Interface Sci.* **1991**, *142*, 61−73.
(11) Yariv, E. Electro-osmotic flow near a surface charge discontinuity. *J. Fluid Mech.* **2004**, *521*, 181−189.
(12) Khair, A. S.; Squires, T. M. Surprising consequences of ion conservation in electro-osmosis over a surface charge discontinuity. *J. Fluid Mech.* **2008**, *615*, 323−334.
(13) Morse, P.; Feshbach, H. *Methods of Theoretical Physics*; McGraw-Hill: New York, 1953.
(14) Hecht, F. New development in freefem++. *J. Numer. Math.* **2012**, *20*, 251−265.
(15) Levine, S.; Marriott, J.R.; Neale, G.; Epstein, N. Theory of electrokinetic flow in fine cylindrical capillaries at high zeta-potentials. *J. Colloid Interface Sci.* **1975**, *52*, 136−149.
(16) Happel, J.; Brenner, H. *Low Reynolds Number Hydrodynamics: With Special Applications to Particulate Media*; Noordhoff International Publishing: Leiden, The Netherlands, 1973.
(17) Sherwood, J. D.; Stone, H. A Electrophoresis of a thin charged disc. *Phys. Fluids* **1995**, *7*, 697−705.
(18) Dagan, Z.; Weinbaum, S.; Pfeffer, R. An infinite-series solution for the creeping motion through an orifice of finite length. *J. Fluid Mech.* **1982**, *115*, 505−523.
(19) Singer, A.; Norbury, J. A Poisson−Nernst−Planck model for biological ion channels — an asymptotic analysis in a three-dimensional narrow funnel. *SIAM J. Appl. Math.* **2009**, *70*, 949−968.
(20) *OpenFOAM - The Open Source CFD Toolbox - User's Guide*, 2nd ed.; OpenCFD Ltd.: Bracknell, United Kingdom, 2012.
(21) Ferziger, J. H.; Perić, M. *Computational Methods for Fluid Dynamics*; Springer-Verlag: New York, 2002.
(22) Murtsovkin, V. A. Nonlinear flows near polarized disperse particles. *Colloid J.* **1996**, *58*, 341−349.
(23) Squires, T. M.; Bazant, M. Z. Induced-charge electro-osmosis. *J. Fluid Mech.* **2004**, *509*, 217−252.
(24) Thamida, S. K.; Chang, H. C. Nonlinear electrokinetic ejection and entrainment due to polarization at nearly insulated wedges. *Phys. Fluids* **2002**, *14*, 4315−4328.
(25) Park, S. Y.; Russo, C. J.; Branton, D.; Stone, H. A. Eddies in a bottleneck: an arbitrary Debye length theory for capillary electro-osmosis. *J. Colloid Interface Sci.* **2006**, *297*, 832−839.
(26) Mao, M.; Ghosal, S.; Hu, G. Hydrodynamic flow in the vicinity of a nanopore induced by an applied voltage. *Nanotechnology* **2013**, *24*, 245202.
(27) Laohakunakorn, N.; Gollnick, B.; Moreno-Herrero, F.; Aarts, D.; Dullens, R.; Ghosal, S.; Keyser, U. F. A Landau−Squire nanojet. *Nano Lett.* **2013**, *13*, 5141−5146.
(28) Keyser, U. F.; Koeleman, B. N.; van Dorp, S.; Krapf, D.; Smeets, R.; Lemay, S.; Dekker, N.; Dekker, C. Direct force measurements on DNA in a solid-state nanopore. *Nat. Phys.* **2006**, *2*, 473−477.
(29) Garaj, S.; Hubbard, W.; Reina, A.; Kong, J.; Branton, D.; Golovchenko, J. Graphene as a subnanometre trans-electrode membrane. *Nature* **2010**, *467*, 190−193.

(30) Schneider, G. F.; Kowalczyk, S.; Calado, V.; Pandraud, G.; Zandbergen, H.; Vandersypen, L.; Dekker, C. DNA translocation through graphene nanopores. *Nano Lett.* **2010**, *10*, 3163−3167.

(31) Merchant, C.; Healy, K.; Wanunu, M.; Ray, V.; Peterman, N.; Bartel, J.; Fischbein, M.; Venta, K.; Luo, Z.; Johnson, A.; Drndić, M. DNA translocation through graphene nanopores. *Nano Lett.* **2010**, *10*, 2915−2921.